Techniques for Doppler spectrum analysis of coherent backscatters within the high-latitude ionosphere

comprehensive study of SuperDARN Doppler spectrum (I)

Solar-Planetary Electromagnetism Lab., Department of Geophysics, Kyoto Univ., Japan
Keisuke Hosokawa (hosokawa@kugi.kyoto-u.ac.jp)

1 Introduction

Super Dual Auroral Radar Network (SuperDARN) is an international collaborative project based on the network of coherent HF radars located in the high-latitude zones of the Northern and Southern Hemispheres (Greenwald *et al.*, 1995). A number of parameters can be estimated from Doppler spectrum obtained form SuperDARN observations. There are three that are important for the purpose of the study of the ionospheric plasma. They are (1) the intensity of the backscatter signal, (2) the mean Doppler velocity (velocity), and (3) the width of the Doppler power spectrum (Figure 1). A relationship between these parameters and original Doppler spectrum is presented in Figure 2. Doppler velocity is widely utilized as a diagnostic of the bulk plasma motion of the ionosphere under the influence of the convection electric field. We have focused on a characteristics of the Doppler spectral width obtained from the SuperDARN radars and have reported that the spectral width is also useful for the identification of the geophysical boundary within the dayside (Hosokawa *et al.*, 2002a, b) and nightside (Woodfield *et al.*, 2002a, 2002b) ionosphere. Now, we are about to carry out a more detailed analysis of a relationship between form of the Doppler spectra and geophysical regimes in the next stage (preliminary result has been obtained already). In the course of this study, further detailed knowledge on the Doppler spectrum analysis is needed. However, our current understanding on the analysis technique of the radar Doppler spectrum is rather poor, which motivates me to review the techniques for the Doppler spectral analysis applied for the data production in the SuperDARN community. Section 2 is devoted to a brief introduction of the radar facility and operation. Main part of this report is section 3 that contains descriptions of the Doppler spectrum analysis technique applied for the SuperDARN radar backscatter echoes.

The aim of this report is just to summarize the observation technique and data processing procedures used in the SuperDARN community. Current status of the SuperDARN Doppler spectrum investigation (I and colleagues are now trying to do!) will be presented in the next colloquium (June 24, 2002).

2 Operation of the Radars (Macroscopic View)

2.1 Ionospheric Backscatter

The high-latitude ionosphere contains a large number of field-aligned plasma irregularities (FAIs) ranging in scale size from a few centimeters to tens of kilometers. Because of the high mobility of the electrons along the direction of the magnetic field line, the density irregularities are field aligned. To produce coherent backscatter, the separation of the FAIs along the radar beam must be half the radar wave length (Bragg condition). For typical HF radars, this corresponds to a separation of between 5 and 25 m. These FAIs are produced by a number of processes such as the gradient

drift and the two-stream instability mechanisms. The maximum backscatter power occurs when the ray direction is perpendicular to the magnetic field lines and the backscatter power is proportional to $(\delta N)^2$ where δN is the level of the fluctuation in the electron density. The motion of the irregularities is dependent on the convection flow, thus a Doppler frequency shift imposed on the backscattered signal is related to the line-of-sight component of the convective flow of the plasmas.

2.2 Sounding System and Operation

The radars of the SuperDARN conform to the basic operating design of the first facility which was built at Goose Bay in 1983. A detailed description of the Goose Bay radar has been given by Greenwald *et al.* (1985). The radars can operate at specific frequencies within the range 8MHz to 20MHz and hence can achieve backscatter from irregularities with wavelengths between 7.5 - 18.75m (Bragg condition). The operating frequency is typically set around 10 MHz, which corresponds to a wavelength of the scattering plasma irregularities of 15m. The radar sounds along 16 different beam directions, separated by 3.24° in azimuth. The radar scans through 16 azimuthal beams in every two minutes and the dwell time on each beam is typically $7sec$ in the current version of the standard common mode operation. Each beam is separated into 75 range gates, usually of 45km in length, with a distance to the first gate of 180km, giving a maximum range of 3555km.

3 Pulse Scheme and Data Processing

3.1 Extraction of Doppler Component (in analog part)

Frequency of the electromagnetic waves used in the SuperDARN observation is ranging from 8MHz to 20MHz, normally set to around 10MHz. Typical drift velocity of ionospheric plasma within the polar F-region ionosphere is an order of $10^1 - 10^3 ms^{-1}$. Corresponding Doppler shift imposed on the backscattered signal ranges from 0.7Hz to 70Hz when the frequency of the transmitted wave is assumed to be 10MHz. Information that is essential for the estimation of ionospheric plasma drift is the Doppler frequency, then, component of the Doppler frequency must be extracted within the receiver before sampling (i.e. before digitalization). Let us assume that form of the transmitted wave, S_T, and that of the received wave, S_R, are

$$S_T = A_T \sin(\omega_0 t + \phi_0) \tag{1}$$

$$S_R = A_R \sin((\omega_0 + \omega_d)t + \phi_1) \tag{2}$$

where ω_0 is angler frequency of the transmitted wave, ω_d is a Doppler shift imposed on the received wave, ϕ_0 and ϕ_1 are initial phase of the transmitted and received wave, respectively. These equations are on the assumption that the Doppler frequency ω_d is unique (in general the Doppler shift of backscattered signal from the ionospheric FAIs is not unique, hence they should be integrated in practice). Here, let us consider a product $S_R \cdot \sin\omega_0 t$,

$$S_R = A_R \sin((\omega_0 + \omega_d)t + \phi_1) \times \sin\omega_0 t \tag{3}$$

$$= \frac{1}{2} A_R [\cos(2\pi f_d t + \phi_1) - \cos((4\pi f_0 + 2\pi f_d)t + \phi_1)] \tag{4}$$

where f_0 is frequency of the transmitted wave and f_d is the Doppler frequency. Since difference in frequency between the first and second term of Eq. (4) is enough large, $A_R \cos(\omega_d t + \phi_1)$, which has an information on ω_d, can be extracted using a bandpass filter in an analog circuit. In a similar

manner, a product $S_R \cdot \cos\omega_0 t$ provides us $A_R \sin(\omega_d t + \phi_1)$. These signals are sampled with a period of $300\mu sec$ as I-component (in phase) and Q-component (quadrature phase), respectively. After this digitalization, we process a complex value, $S(t)$, composed of I and Q-component,

$$S(t) = I + iQ \tag{5}$$
$$= A_R \cos(\omega_d t + \phi_1) + iA_R \sin(\omega_d t + \phi_1) \tag{6}$$
$$= A_R exp^{i(\omega_d t + \phi_1)} \tag{7}$$

Derivation of the I and Q-component is schematically illustrated in Figure 3.

3.2 Calculating Auto Correlation Function (ACF)

There exist various methods for an analysis of time-series variations with periodic or quasi-periodic characteristics (e.g., Fourier analysis, maximum entropy method, wavelet analysis, auto correlation function analysis, etcetera). SuperDARN radars transmit electromagnetic waves toward the ionosphere and receive time-series variation of the signals backscattered from the plasma irregularities, in which signal processing technique is based on auto-correlation function (ACF) analysis. There is no easy way to understand the detail of the SuperDARN data production without knowledge of the ACF analysis. In this section, essence of the ACF analysis is briefly introduced, and how it is applied for the radar signal processing is also presented.

3.2.1 Brief Tutorial for Spectrum Analysis Using ACF

If we consider a single time-series $S(t)$, auto-correlation function (ACF) can be defined as an ensemble average of the product $S(t) \cdot S(t+\tau)$

$$\mathrm{ACF}(\tau) = < S(t) \cdot S(t+\tau) > \tag{8}$$
$$= \lim_{T\to\infty} \frac{1}{T} \int_{-T/2}^{T/2} S(t) \cdot S(t+\tau)\ dt \tag{9}$$

where the bracket means ensemble average (it can be replaced with temporal average: Ergodic hypothesis) and τ is a lag. What is worth noting is that the ACF is not a function of t and a function of lag τ. When the time-series considered is continuous and is defined from -∞ to ∞, one can use ACF normalized by a value of zero lag ACF instead of ACF, which is called auto-correlation function coefficient (here we name it $ACFC$). If we consider $\sin\omega t$ for example, corresponding ACF coefficient can be obtained as follows:

$$\mathrm{ACFC}(\tau) = \lim_{T\to\infty} \int_{-T/2}^{T/2} \sin\omega t \cdot \sin\omega(t+\tau)\ dt \ /\ \lim_{T\to\infty} \int_{-T/2}^{T/2} \sin\omega t \cdot \sin\omega t\ dt \tag{10}$$
$$= \cos\omega\tau \tag{11}$$

When one consider the ACF of non-continuous time-series data, the ACF can be defined as a summation,

$$\mathrm{ACF}(\tau) = \frac{1}{N} \sum_{n=1}^{N} S(t_n) \cdot S(t_n + \tau) \tag{12}$$

Figure 4 demonstrates one of the simplest examples. The top panel shows original sine wave with frequency of 5Hz (i.e., $\sin 10\pi t$) where averaged power is presented as a shadow. The middle panel

is a corresponding ACF ($1/2\cos 10\pi t$). Comparison between these two curves provides us physical meaning of the ACF, that is, the ACF has its maximum when the lag is equal to an integer multiple of the period of original time-series. The other thing important is that Fourier transform of the ACF is a power spectrum of the original time-series. This fact is well known as Wiener-Khintchine's formula and widely utilized in the spectrum analysis. The bottom panel of Figure 4 gives a Fourier transformation of the ACF shown in the middle panel. Frequency of the original wave (5Hz) is obtained and its power is also consistent with the averaged power of the original wave. The other example is shown in Figure 5, which is slightly complicated. Original wave is a summation of the waves whose frequencies are 5 and 10Hz. Also in this case, we can see that the ACF analysis reaches correct answer (i.e., two peaks can be found at 5 and 10Hz).

3.2.2 Single Pulse Observation

Multipulse observation (coded pulse) is employed in the SuperDARN observation. However, we start with the description of single pulse observation for better understanding, and then we will turn to the multipulse observations actually used in the SuperDARN observations. Here, single pulse means HF band (8MHz - 20MHz, period is about $0.1\mu sec$) electromagnetic wave whose length is approximately $300\mu sec$ (containing 3000 periods). Signal is sampled as a form of the IQ-output with a period of $300\mu sec$,

$$S(t) = A\exp^{i\omega_d t}\exp^{i\phi_1} \tag{13}$$

Figure 6 schematically illustrates a travel of the transmitted waves. Range from which the received signal comes can be determined from arrival time. Actually, a number of single pulses are needed for the calculation of the ACF, hence one set of single pulse scheme contains large number of the single pulses (70 subsets). In addition, interval between the pulses should vary in order to calculate ACF for various lags. When the set of single pulses is completed, we can turn to calculate ACF of accumulated IQ-output for each range gates for various lags. Since the IQ-output is a complex form, then the ACF of $S(t)$ is,

$$\begin{aligned} ACF(r,\tau) &= < S(r,t)\cdot S(r,t+\tau)^* > & (14)\\ &= < A(r)\exp^{i(\omega_d(r)t+\phi_1(r))}\cdot A^*(r)\exp^{-i(\omega_d(r)t+\omega_d(r)\tau+\phi_1(r))} > & (15)\\ &= A(r)\cdot A^*(r)\exp^{-i\omega_d(r)\tau} & (16)\end{aligned}$$

Once the ACF is calculated, we can employ Wiener-Khintchine's formula and obtain the power spectrum from the Fourier transformation of the ACF.

3.2.3 Correlation Time

Single pulse observation seems to be valid for the observation of the ionospheric plasma drift. In practice, however, this kind of pulse scheme is never employed in the observation of the backscatter echoes from the FAIs. Here, we introduce a concept of correlation time and discuss the reason why the single pulse observation is never used in our observations. Correlation time is defined as an interval during which correlation caused by common physical factor is maintained in time-series data. ACF analysis is based on a correlation between two points in the single time-series. If the sampling period is larger than the correlation time, we can not obtain substantial power spectra from the ACF analysis. In our case, this correlation time is corresponding to the interval during which the nature of the

scattering medium in the ionosphere is preserved. Typical correlation time of the FAIs within the high-latitude E and F region ionosphere ranges approximately 2-30$msec$. Physically, it may be due to the finite lifetime of the individual irregularity structures and the random or turbulent velocities that exist in the scattering volume. If we try to obtain backscatter echo over the horizon (i.e. 3000km in range), sequence of the single pulse must appropriate 20$msec$. This could be longer than the correlation time of the scattering medium, then ACF with effective lag will not be obtained. If we apply ACF analysis for Doppler spectrum derivation, temporal resolution of the sampling should be much shorter than the correlation time of the scattering volume we expect.

3.2.4 Multiple Pulse Observation

The basic principle is to transmit a sequence of pulses such that the time delays between any two pulses of the sequence are different and form a regular series. This pulse scheme was initially proposed by Farley (1969) and precisely described by Farley (1972). One of the multipulse schemes currently used by the SuperDARN radars (7-pulse scheme) is shown in Figure 7. The pulse length is 300μsec, giving a resolution of 45km in radar range. When receiving, the radar signal is digitized with a sampling period of 300μsec, equal to the pulse length. The time separation between pulses is an integer multiple of $\tau_0 = 2.4\ msec$ (equal to 8 sampling periods). From the 7-pulse sequence, 17 delays of the ACF are calculated. The total signal received at a given time is the sum of the signals backscattered from different range gates and corresponding to the pulses previously transmitted. For instance (illustrated in Figure8), 33$msec$ after the start of the pulse sequence, the received signal will be the sum of the echoes backscattered at ranges 1710km (from the second pulse of the sequence) and 630km (from the third pulse). The echo backscattered from the range 4950km (first pulse) can be neglected, because echoes returning from ranges over 3500km are usually too faint. The received signal can be written,

$$S_0 = A_1 \exp^{i\omega_1 t_0} + A_2 \exp^{i\omega_2 t_0} \exp^{i\phi_2} \tag{17}$$

where t_0 is the time of the measurement (in this case, 33$msec$), ω_1 and ω_2 are the angular frequencies of the signals backscattered from ranges 1710 and 630km, respectively, and A_1 and A_2 are the associated amplitudes. The phase ϕ_2 is the phase difference between two signals. In order to calculate the ACF for the range 1710km and for the delay τ (for instance, $\tau = 3\tau_0$), we use also the signal received at time $t_0 + \tau$ (here 40.2$msec$),

$$S_\tau = A_1^{'} \exp^{i(\omega_1 t_0 + \tau)} + A_3 \exp^{i\omega_3 (t_0+\tau)} \exp^{i\phi_3} \tag{18}$$

This signal is also the sum of two echoes, one from the range 1710km with the amplitude $A_1^{'}$ (which can be different from A_1 because of the time variation of the scattering fluctuations), and one from the unwanted range 2790km with the amplitude A_3 and angular frequency ω_3, in which phase difference between two sources is represented by ϕ_3. The product $S_0 \cdot S_\tau^*$ is then,

$$\begin{aligned} S_0 \cdot S_\tau^* = & A_1 A_1^{'*} \exp^{-i\omega_1 \tau} \\ & + A_2 A_1^{'*} \exp^{-i(\omega_1 - \omega_2) t_0} \exp^{-i\omega_1 \tau} \exp^{-i\phi_2} \\ & + A_1 A_3^{'*} \exp^{-i(\omega_3 - \omega_1) t_0} \exp^{-i\omega_3 \tau} \exp^{-i\phi_3} \\ & + A_2 A_3^{'*} \exp^{-i(\omega_3 - \omega_2) t_0} \exp^{-i\omega_3 \tau} \exp^{-i(\phi_3 - \phi_2)} \end{aligned} \tag{19}$$

This relation is valid for a single multipulse sequence. Only the first term in the right-hand side of Eq. (19) represents the ACF for the range 1710km and the delay $3\tau_0$. The three remaining terms are

cross products between different ranges. Their relative amplitude is reduced by repeating the multiple scheme. The phases ϕ_i are random variables, due to the incoherence of the phase of the fluctuations which are responsible for the backscatter, at times separated by the delay between successive multipulse sequences., typically $88.8 msec$. The damping of these terms is proportional to $N^{1/2}$, where N is the number of multipulse sequences. A relative damping of 8.6 is obtained when the ACF is averaged over 75 multipulses. From here on, only the first term in Eq. (19) will be considered.

$$\mathrm{ACF}(\tau) = < S_0 \cdot S_\tau^* > = < A_1 A_1^{'*} \exp^{-i\omega_1 \tau} > \tag{20}$$

This technique allows us to obtain 17 points of the complex ACF in each of the 75 range gates for each multipulse sequence. During the 7 s when the radar is transmitting on a specific beam, there are approximately 75 multipulse sequences transmitted. The 75 successive ACFs are averaged to give one mean ACF for the integration period of that beam (the top and middle panel of Figure 9). As noted before, power spectrum of the radar backscatter can be obtained from Fourier transformation of the obtained ACF (the bottom panel of Figure 9). In the example shown in Figure 9, it is clearly shown that the cross terms in Eq. (19) have no influence on the experimental ACF, thanks to the averaging process.

3.3 Fitted Parameter Derivation

The ACF can be converted into Doppler power spectra by simply performing a Fourier transform on the complex ACF. From this transformation Doppler velocity, Doppler spectral width, and backscattered power can be determined. However, it is more efficient to obtain these parameters directly from the ACF rather than to perform the large number of FFTs. Several studies of the radar Doppler spectrum have shown that the Doppler power spectra generally Lorentzian in shape and the ACF decays exponentially. Being based on these characteristics of the SuperDARN ACFs, it is possible to fit an assumed functional form to each of the ACFs. The procedure of direct parameter derivation from the ACF is introduced in this section.

3.3.1 Noise Reduction

There are several sources of noise which complicate the analysis of the radar data. The cosmic HF background noise is relatively constant in time but has a frequency dependence. The multipulse technique causes strong scatter at some ranges to contribute to the noise at other ranges. In addition, there are local sources of HF noise produced by nearby instrument, as well as the inherent noise of the receiver and digitizers. Finally, in the HF frequency band, there are nearly always remote radio transmitters that contribute to the noise background at varying intensity levels. Some of these transmitters are CW (continuous wave) sources. The first stage of the noise reduction is the determination of the basic noise level and the noise ACF. An initial noise level is determined from the averaged backscattered lag-0 power from the 10 weakest ranges. An average noise ACF is then formed from all the ACF which have lag-0 power less than 1dB above the initial estimate of the noise level. In a typical case where there are no external transmitters producing noise, the noise ACF will have a non-zero power at lag-0 and be nearly zero for all other lags. If a CW transmitter is present, however, it will be present at all range gates. In this case, the noise ACF will show a clear non-zero frequency. In either case, the noise ACF is then subtracted from the raw ACFs. This noise reduction process is shown in Figure 10.

3.3.2 Doppler Velocity

The velocity is derived from the Doppler frequency, deduced from the phase of the ACF by a linear least squares fit. The phase ϕ is given by

$$\phi = arctan(\mathrm{Img}(\mathrm{ACF}(\tau))/\mathrm{Real}(\mathrm{ACF}(\tau))) = \omega_d \tau \pm 2n\pi \tag{21}$$

A typical example taken from the SuperDARN radar is shown in Figure 11. Once the curve of phase and lag is fitted and then ω_d is obtained, corresponding Doppler velocity is easily estimated using

$$V_d = \frac{c}{2\omega_0}\omega_d \tag{22}$$

where c is the velocity of light and ω_0 is the transmitter frequency.

3.3.3 Backscatter Power and Doppler Spectral Width

Baker *et al.* (1988) demonstrated that the ACF of the radar backscattered signal can be characterized as a sinusoidal wave in an exponentially decaying envelope. Additional studies of the spectral shapes of the radar Doppler spectrum by Villain *et al.* (1987) and Hanuise *et al.* (1993) pointed out that the Doppler power spectra are generally Lorentzian in shape and the ACF decays exponentially. Then, the Doppler spectral width and backscattered power can be deduced from the time variation of the power of the ACF

$$P = (R^2 + I^2)^{1/2} \tag{23}$$

If the spectra are assumed to be Lorentzian, power of the ACF is characterized as an exponential profile with the damping factor α

$$|\mathrm{ACF}(\tau)| = B\ exp^{-\alpha\tau} \tag{24}$$

Once least-square fit is performed, width of the Lorentzian spectrum is automatically derived

$$w = \frac{c}{\omega_0}\alpha \tag{25}$$

B is the backscattered power, which is consistent with lag-0 power ideally. This procedure is shown in Figure 12. There is two exceptions to this rule. Very narrow spectra observed in the E-region often appear to be more characteristics of a Gaussian shape (Milan *et al.*, 2000, 2001) and spectra in the cusp region are broad and typified by multiple Gaussian components (Baker *et al.*, 1995).

4 Outstanding Problems

⋆ Multiple spectrum

Method for separating multiple component echoes using high-resolution spectral analysis was developed by Barthes *et al.* (1998). But, this function is not installed on-site data processing.

⋆ Phase aliasing in Doppler velocity determination

No one knows whether the phase aliasing often occurs or not. However, comparison of the velocities obtained from SuperDARN and other radar facility (e.g., EISCAT) is really good (e.g., Hosokawa *et al.*, 2002). This allows us to use the Doppler velocity obtained from the SuperDARN radar as a drift velocity of the ionospheric plasma, keeping in mind the possibility that we may underestimate or overestimate the velocity by a small amount.

Reference

Baker, K. B., R. A. Greenwald, J. P. Villain, and S. Wing, Spectral characteristics of high frequency (HF) backscatter form high latitude ionospheric irregularities: Preliminary analysis of statistical properties, *Interim Rep., RADC-TR-87-284, Rome Air Dev. Cent., Briffis Air Force Base, N. Y.*, 1988.

Baker, K. B., J. R. Dudeney, R. A. Greenwald, M. Pinnock, P. T. Newell, A. S. Rodger, N. Mattin, and C-I. Meng, HF-radar signatures of the cusp and low latitude boundary layer, *J. Geophys. Res., 100,* 7671, 1995.

Farley, D. T., Incoherent scatter correlation function measurements, *Radio Sci., 4*, 935-953, 1969.

Farley, D. T., Multiple-pulse incoherent-scatter correlation function measurements, *Radio Sci., 7*, 661-666, 1972.

Greenwald, R. A., K. B. Baker, R. A. Hutchins, and C. Hanuise, An HF phased-array radar for studying small-scale structure in the high-latitude ionosphere, *Radio Sci., 20*, 63-79, 1985.

Greenwald, R. A., et al., DARN/SuperDARN: A global view of the dynamics of high-latitude convection, *Space Sci. Rev., 71*, 761-796, 1995.

Hanuise, C. J. P. Villain, J. C. Cerisier, C. Senior, J. M. Ruohoniemi, R. A. Greenwald, and K. B. Baker, Interpretation of HF radar ionospheric Doppler spectra by collective wave scattering theory, *Annales Geophysicae, 11*, 29-39 2002.

Hosokawa, K., E. E. Woodfield, M. Lester, S. E. Milan, N. Sato, A. S. Yukimatu, and T. Iyemori, Statistical characteristics of Doppler spectral width as observed by the conjugate SuperDARN radars, *Annales Geophysicae, in press*, 2002.

Hosokawa, K., M. Sugino, M. Lester, N. Sato, A. S. Yukimatu, and T. Iyemori, Simultaneous measurement of duskside subauroral irregularities from the CUTLASS Finland radar and EISCAT UHF system, *submitted to J. Geophys. Res.*, 2002.

Hosokawa, K., E. E. Woodfield, M. Lester, S. E. Milan, N. Sato, A. S. Yukimatu, and T. Iyemori, Interhemispheric comparison of spectral width boundary as observed by the SuperDARN radars *submitted to Annales Geophysicae*, 2002.

Milan, S. E., M. Lester, N. Sato, H. Takizawa, and J. P. Villain, Investigation of the relationship between optical auroral forms and HF radar E region backscatter, *Annales Geophysicae, 18*, 608-617, 2000.

Milan, S. E., and M. Lester, A classification of spectral populations observed in HF radar backscatter from the E region auroral electrojets, *Annales Geophysicae, 19*, 189-204, 2001.

Villain, J. P., R. A. Greenwald, K. B. Baker, and J. M. Ruohoniemi, HF radar observation of E region plasma irregularities produced by oblique electron streaming, *J. Geophys. Res., 92*, 12,327-12,342, 1987.

Woodfield, E. E., J. A. Davis, P. Eglitis, and M. Lester, A case study of HF radar spectral width in the post midnight magnetic local time sector and its relationship to the polar cap boundary, *Annales Geophysicae, in press*, 2002.

Woodfield, E. E., K. Hosokawa, S. E. Milan, N. Sato, and M. Lester, An inter-hemispheric, statistical study of nightside spectral width distribution from coherent HF scatter radars, *submitted to Annales Geophysicae*, 2002.

Figures

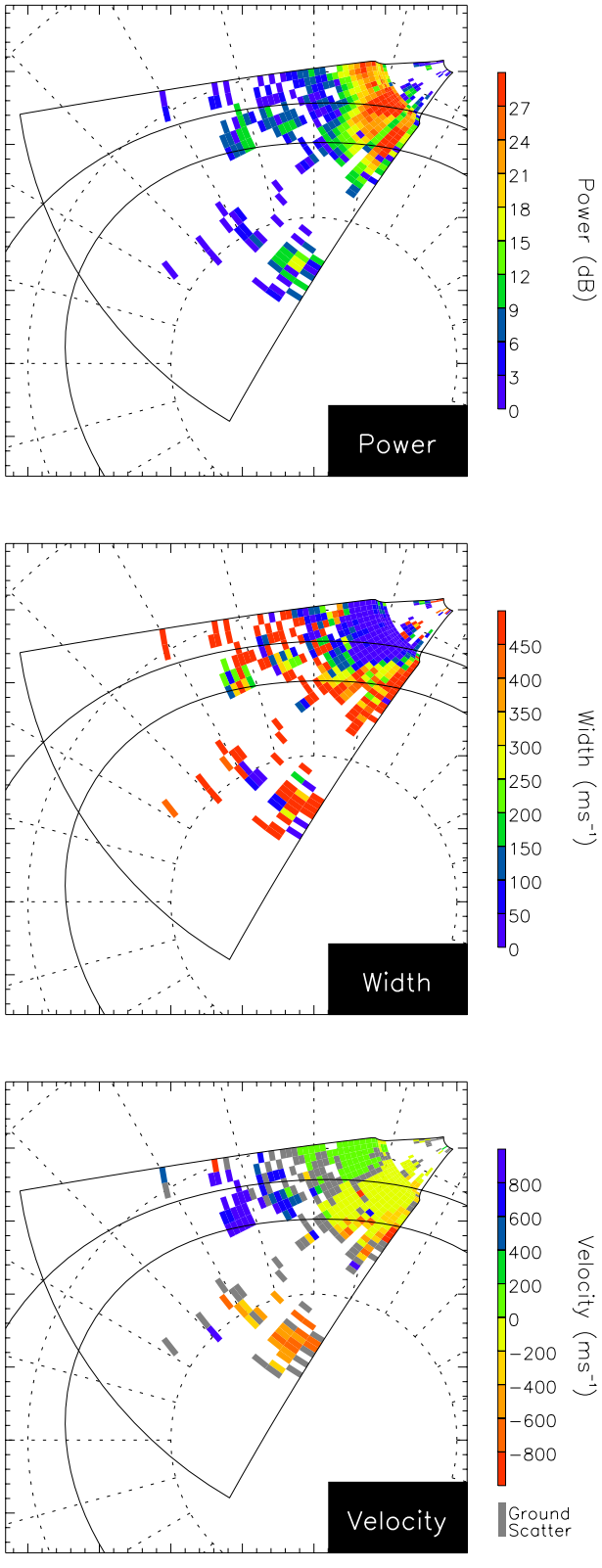

Figure 1. Three fitted parameters, power, width and velocity.

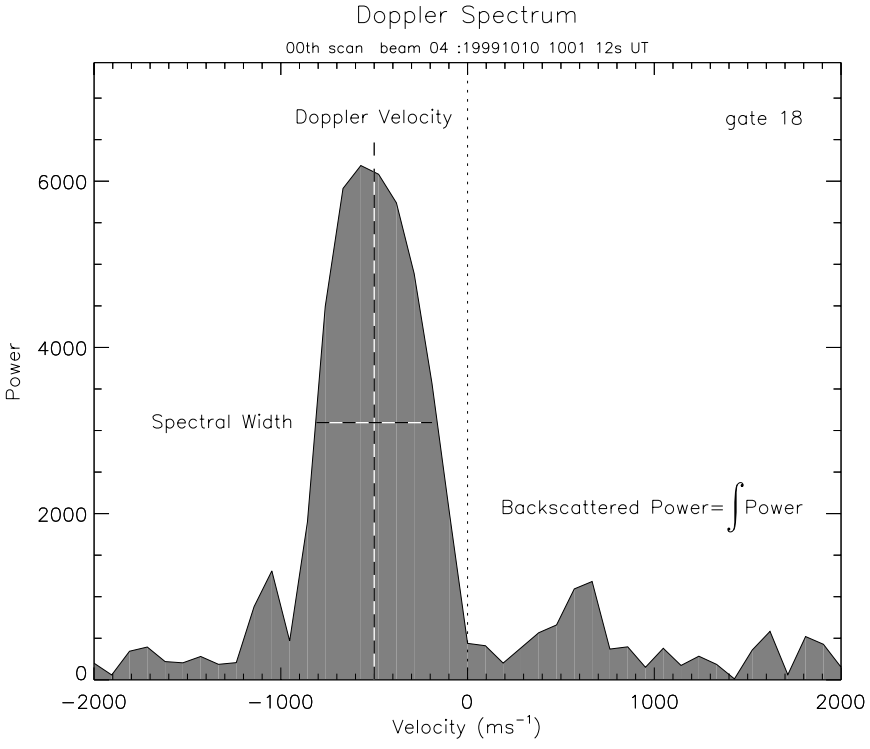

Figure 2. Sample spectrum

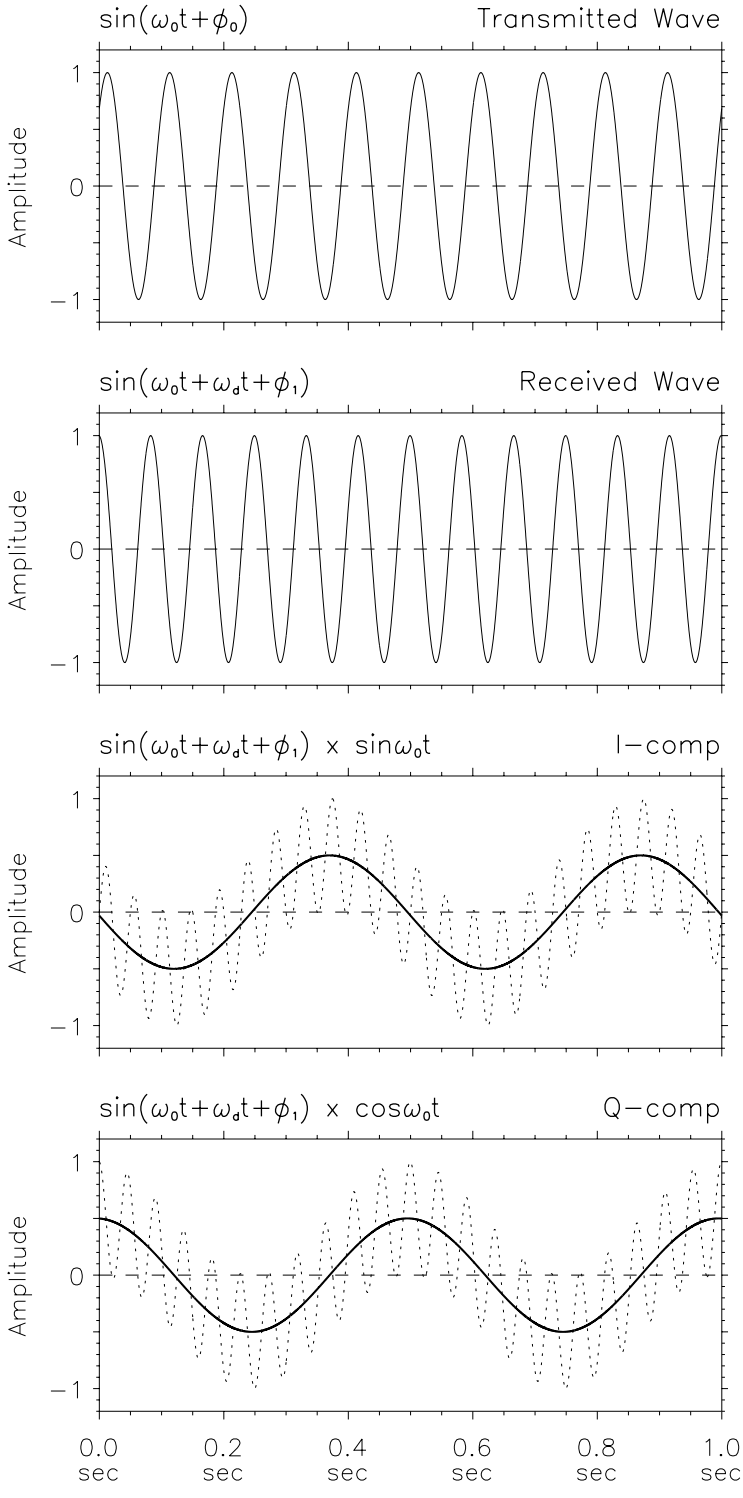

Figure 3. Extraction of the Doppler component.

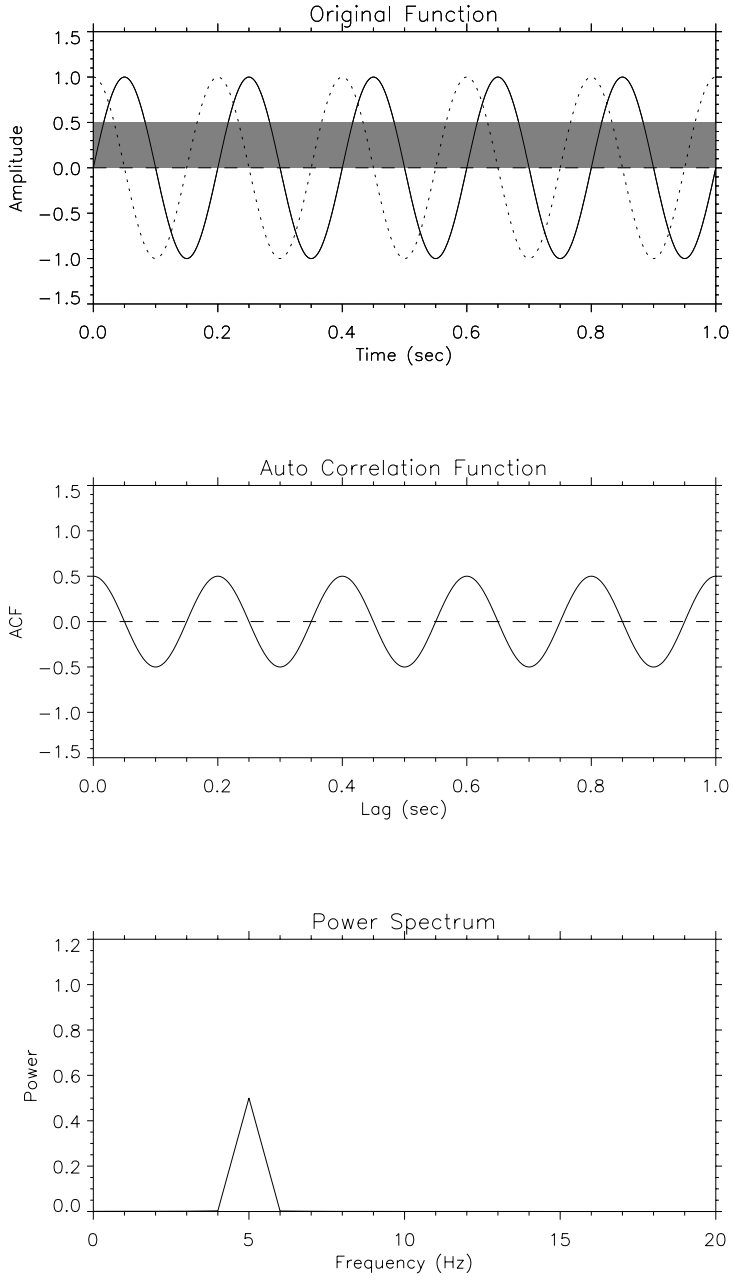

Figure 4. Sample of ACF analysis (1)

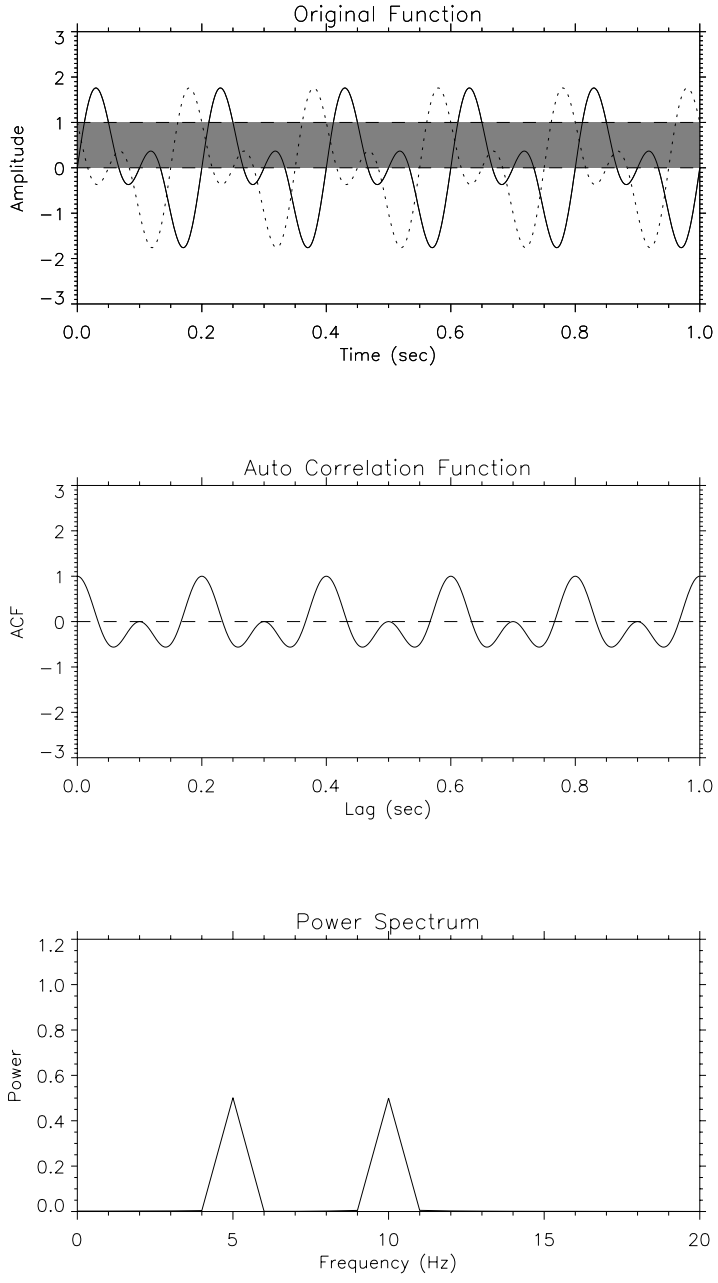

Figure 5. Sample of ACF analysis (2)

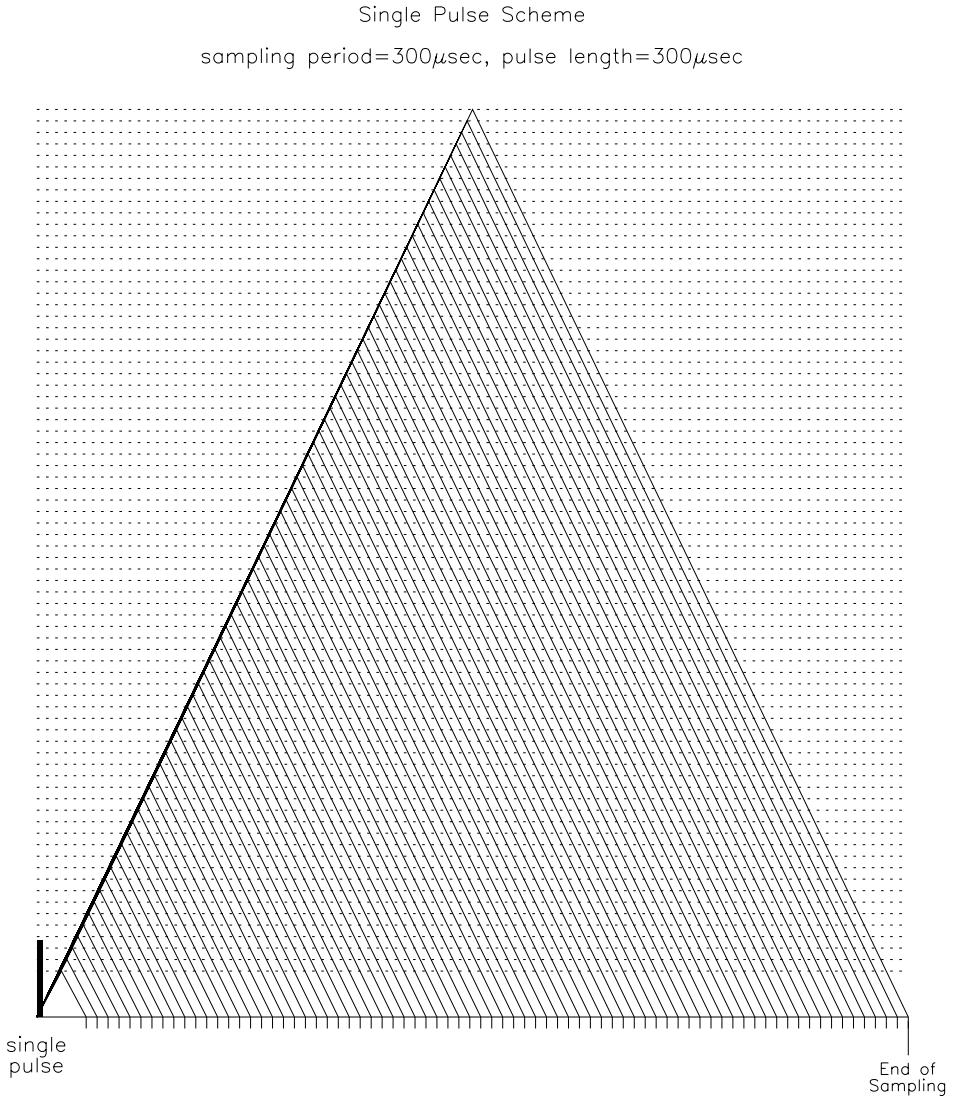

Figure 6. Single pulse scheme.

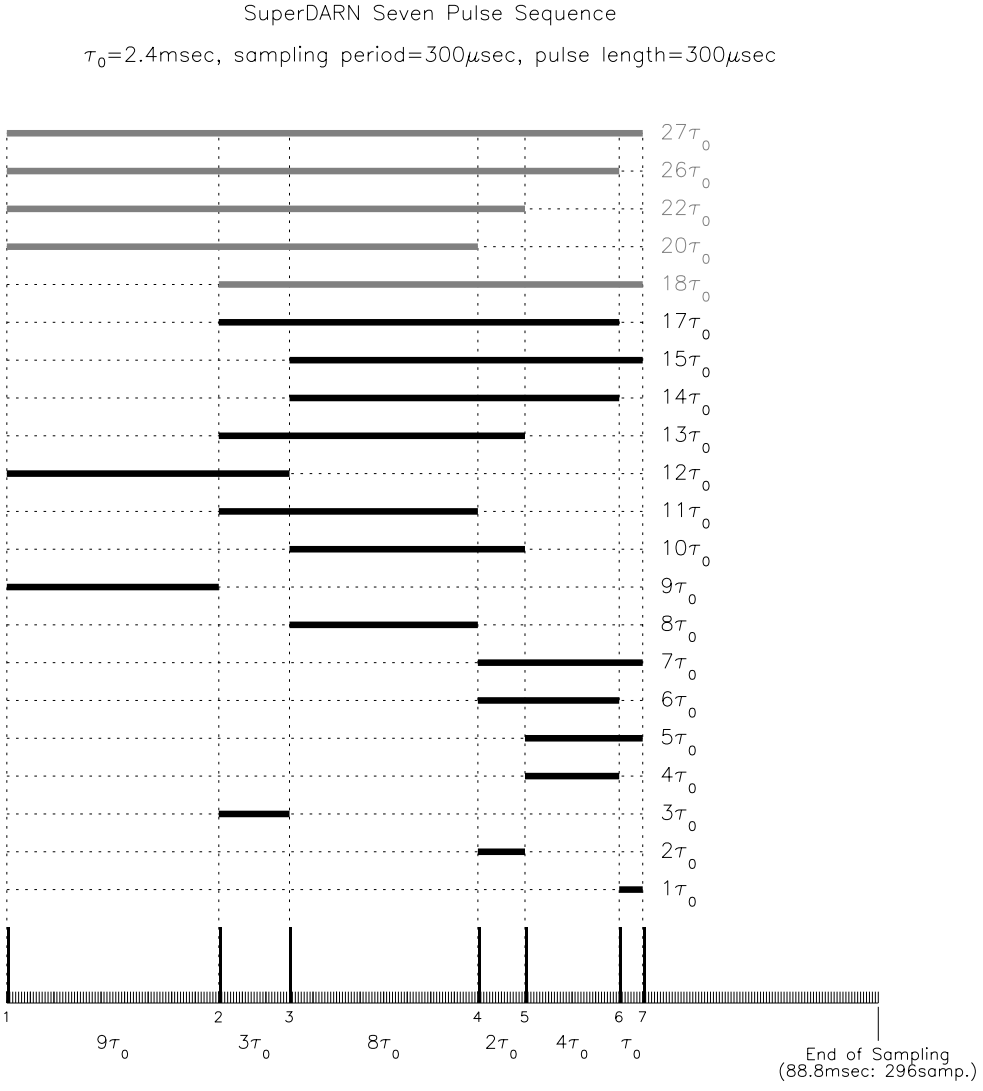

Figure 7. Multi pulse scheme (seven pulse).

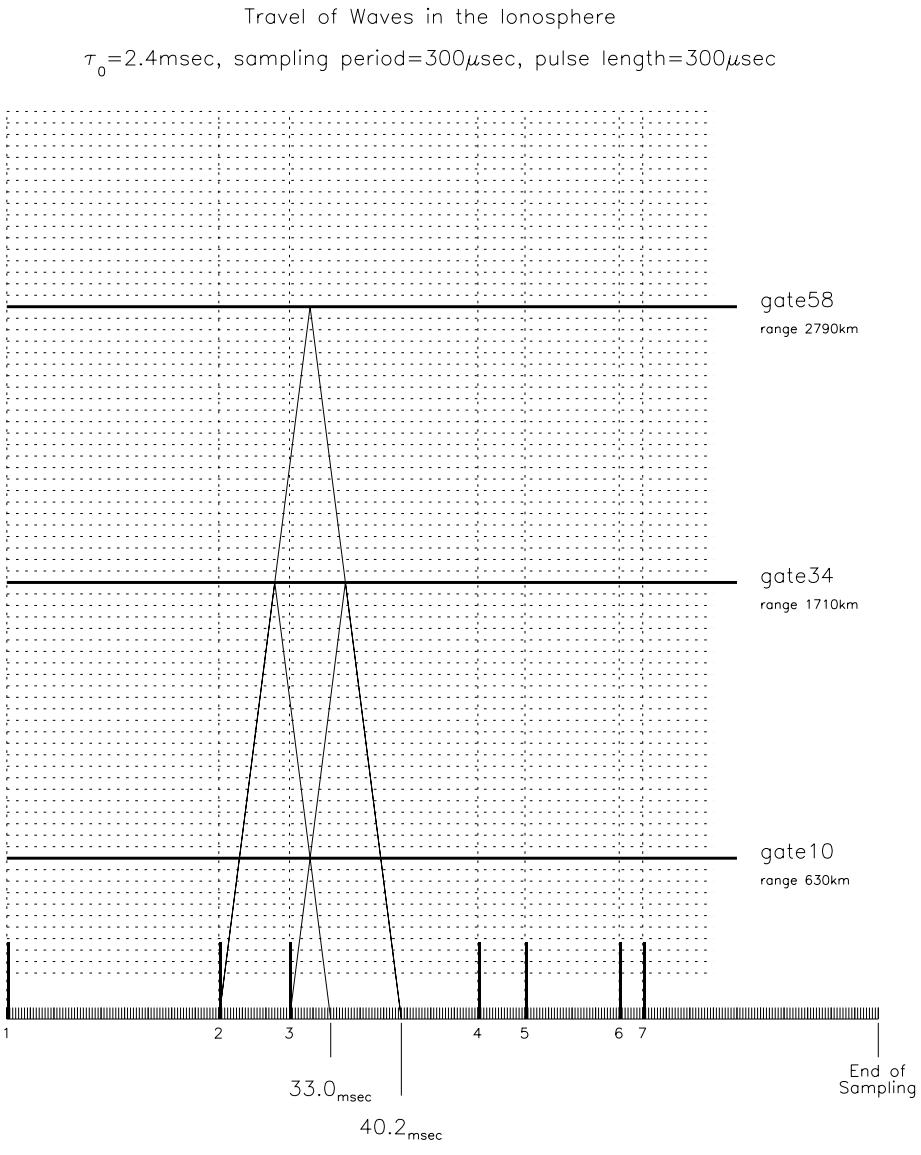

Figure 8. Illustration of traveling transmitted wave.

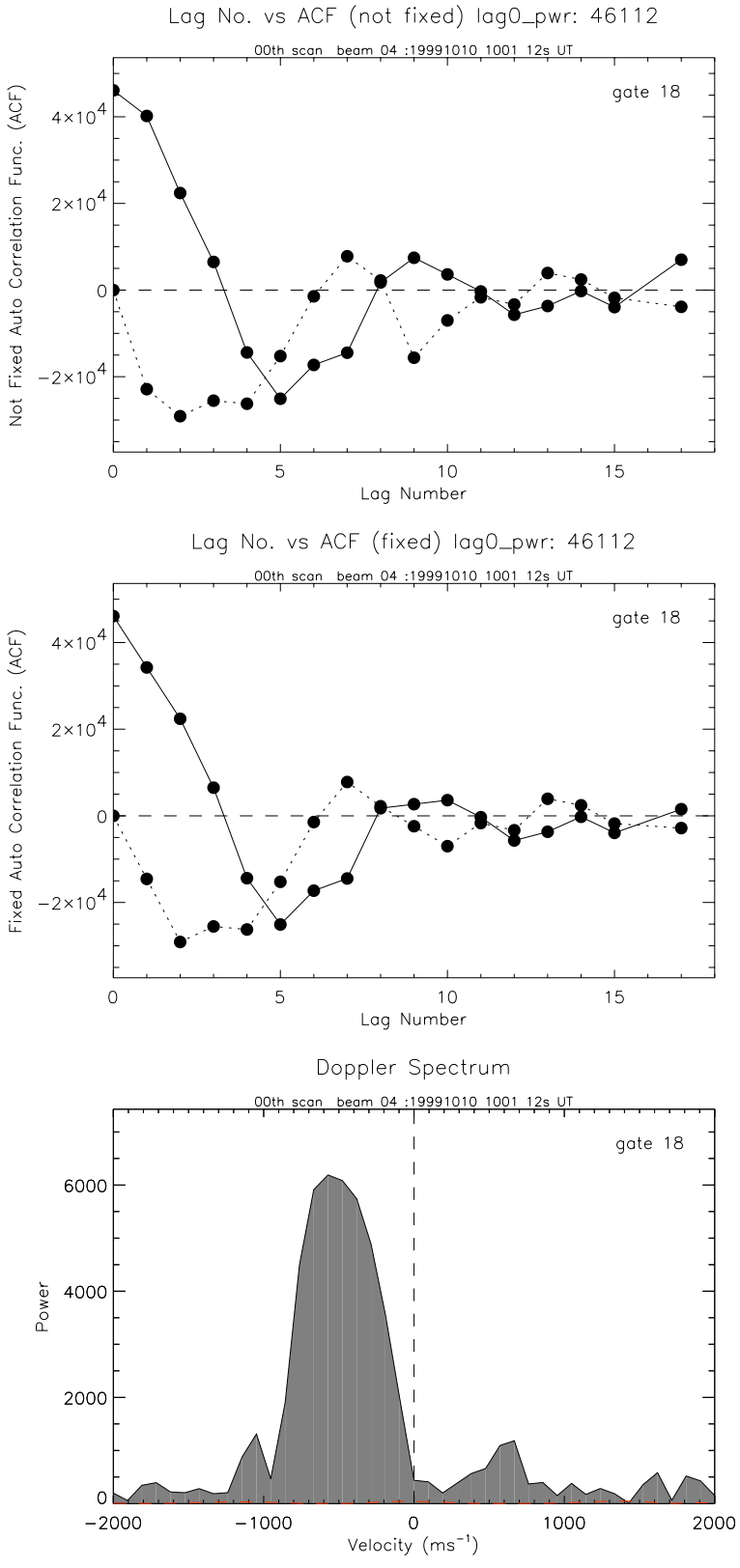

Figure 9. Auto-correlation function and corresponding spectrum.

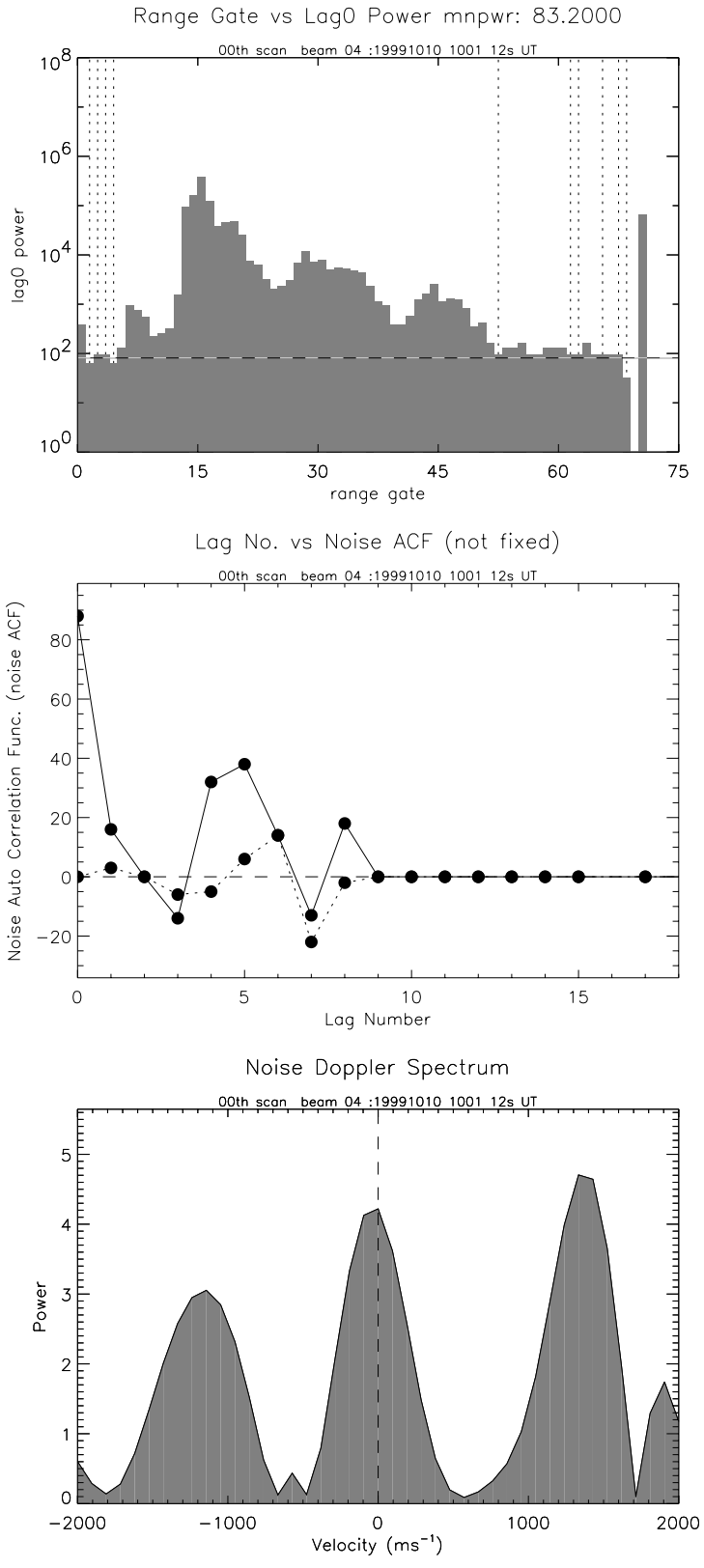

Figure 10. Noise ACF and noise spectrum.

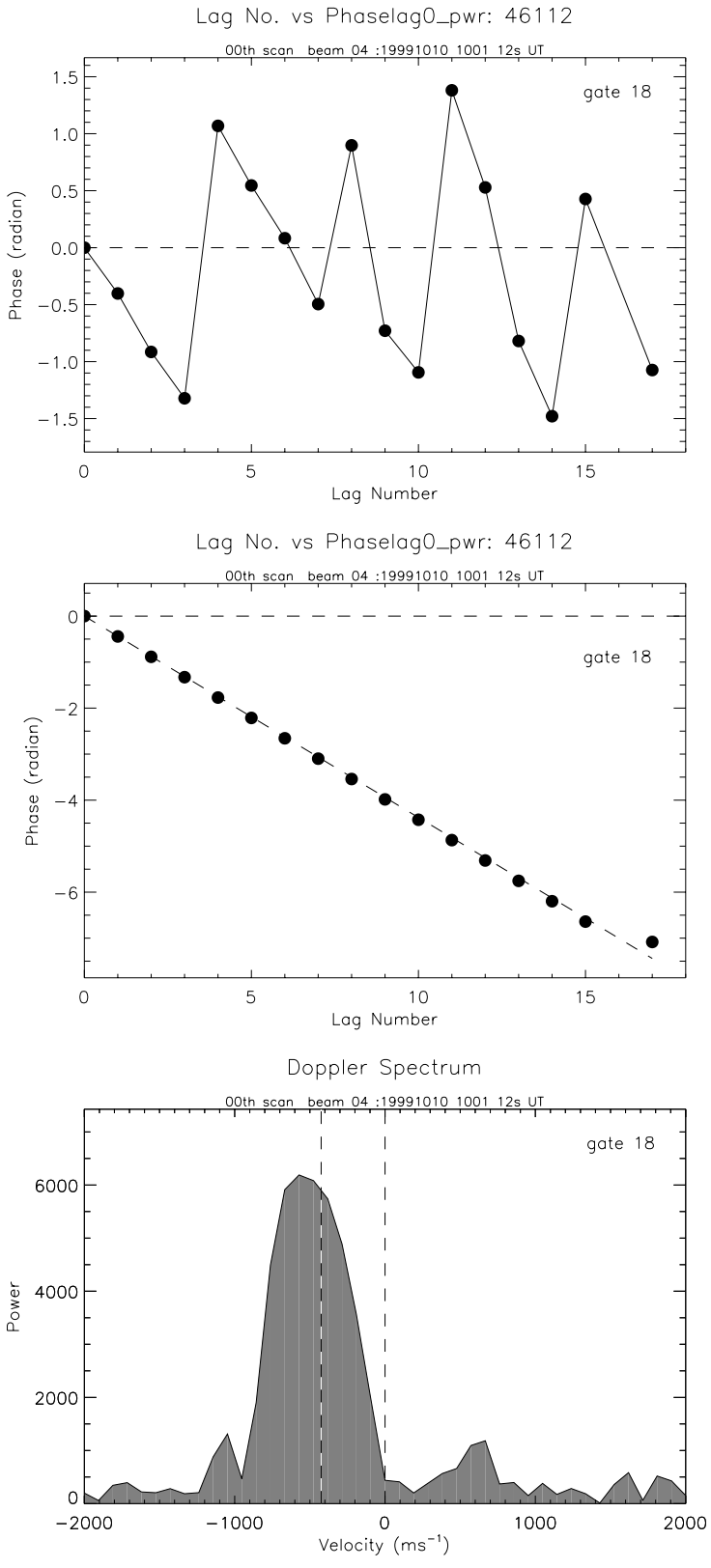

Figure 11. Velocity determination process.

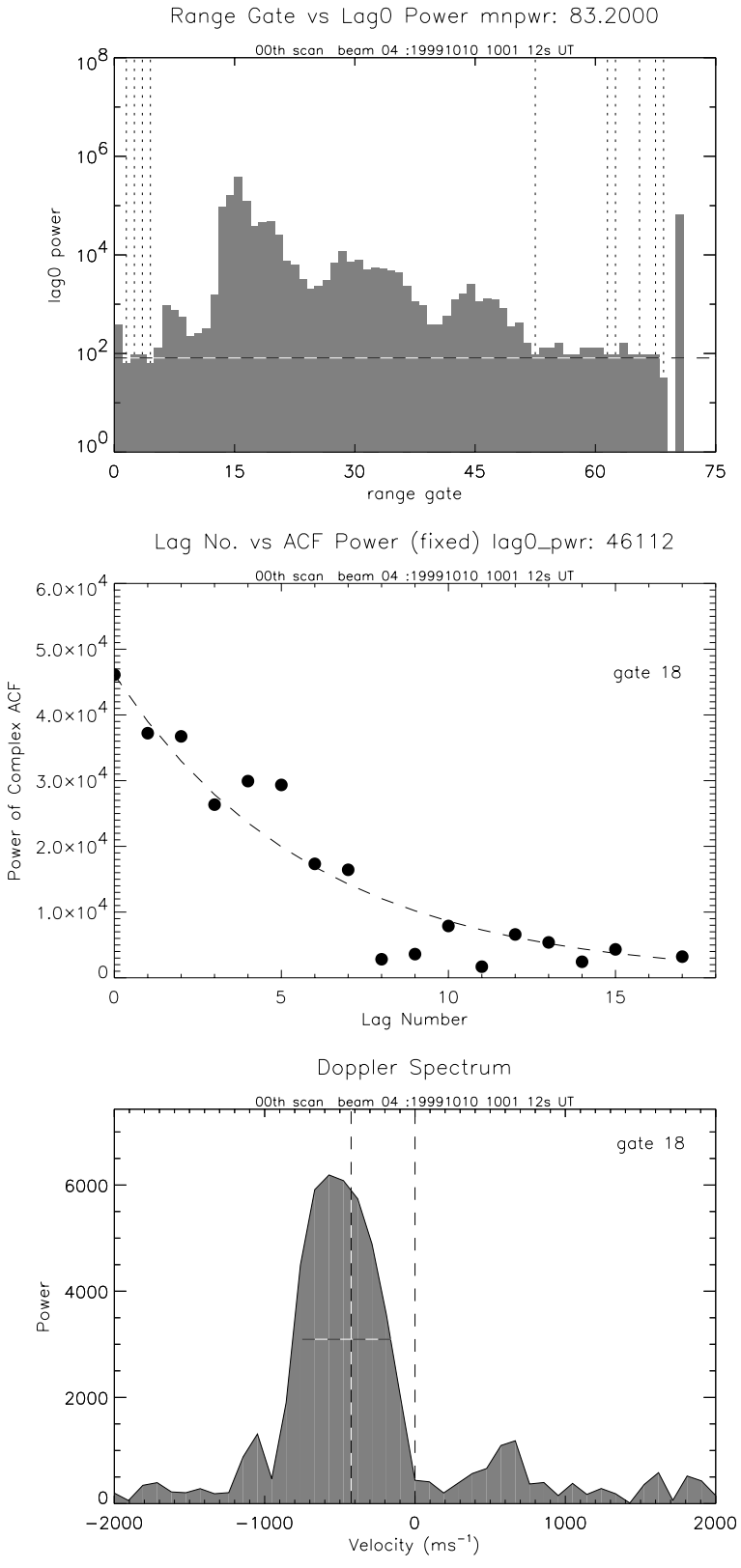

Figure 12. Spectral width determination process.